Compact 2.4 THz 5-Bit Substrate Guided Wave Photonic True-time-delay Module for Phased Array Antennas

Zhenhai Fu, Richard L. Q. Li, and Ray T. Chen
Microelectronics Research Center
Department of Electrical and Computer Engineering
The University of Texas at Austin, Austin, Texas 78758
Tel: 512-4717035; Fax: 512-4718575; E-mail:raychen@uts.cc.utexas.edu

ABSTRACT

Photonic true-time-delay (TTD) lines offer many advantages over their electronic counterparts and attract more and more research efforts. In this paper, we report the demonstration of a 32 TTD lines (5-bit) based on substrate guided wave propagation combined with slanted photopolymer volume phase gratings on a quartz substrate. The system design, device fabrication, optimization of fanout intensity uniformity, and device performance evaluation are addressed as well. The fanout beam intensity uniformity is within ±10%. The packing density is 2.5 delay lines/cm^2. The device has a measured bandwidth of up to 2.4 THz and a measured fanout delay step of 50 ps. A 50GHz optically heterodyned microwave signal is generated, sent through the device, and then detected at the output end.

Keywords-----Phased array antenna, True-time-delay, Hologram, Photopolymer, Substrate guided wave

I. INTRODUCTION

For phased array antennas (PAAs) with only phase shifters, rather than time delay, the antenna pointing direction changes with frequency change as[1, 2]

$$\Delta\Phi = -(\Delta f / f_0)\mathrm{tg}\Phi_0 \quad \text{(rad)}$$

$$\text{or} \quad \Delta\Phi = -57.3(\Delta f / f_0)\mathrm{tg}\Phi_0 \quad \text{(degree)}, \qquad (1)$$

where Φ_0 is nominal pointing direction, f_0 is nominal operation frequency, $\Delta\Phi$ is change in pointing direction for a change in frequency Δf which is shown in Figure 1. This effect increases dramatically as Φ_0 increases. As the beam moves away from the nominal pointing direction with varying frequencies, the gain in the direction Φ_0 decreases. Therefore, such kind of phased array antenna systems have a basic problem of narrow bandwidth. The use of true-time-delays (TTD) instead of phase shifts can give enhanced

SPIE Vol. 3290 • 0277-786X/97/$10.00

bandwidth[3]. For real system implementations of TTD beam steering, it is usually impractical trying to realize a continuously tuned TTD due to the level of complexity in size and high costs. Two methods have been used to produce time-corrected steering in practical phased arrays[4,5]. The first method is to group the array into subarrays, use time-delay device behind each subarray, and use phase shift behind each element as shown in Figure 2. The bandwidth of an array of M subarrays is M times that of the phase-steering array. Second, each time-delay unit is built to provide a discrete set of delay lines rather than continuous delay lines. A higher degree of accuracy can be achieved with a smaller delay step. The antenna can thus be scanned at correspondingly smaller angular increment. In this way, the system provides some, but not all, of the benefits of true-time-delay steering. The progress in photonics technology in recent years has raised great interests in providing true-time-delays using optical means because photonic TTDs can offer a wider bandwidth while keeping a compact size, a reduced weight with very low RF interference[6].Various types of photonic TTD delay units have been demonstrated by a few research groups, such as fiber delay lines[6,7], fiber optic Bragg grating TTD element[8], waveguide optical time-shift network[9,10,11], acousto-optic TTD element[12], and multiwavelength WDM TTD lines[13]. These TTD lines do have some advantages such as accurate time delay and monolithic integration with detectors, but they suffer from some disadvantages such as many light sources, switches and modulators needed, low packing density, complexity in fabrication and control, and high loss.

In our previous papers, we reported a high packing density 3-bit true-time-delay lines devices with a minimum delay step of ~100 ps and a bandwidth of 2.5 THz[14-16]. In this report, the design, fabrication, and evaluation of a 5-bit photonic TTD module with 50 ps delay step is presented. This module combines a 1-to-4 fiber beam splitter with four 1-to-8 collinear guided wave fanouts to provide 32 surface normal fanout beams carrying an optically generated heterodyne signal up to 50 GHz with different delays. A bandwidth of 2.4 THz is confirmed experimentally by femtosecond laser pulse broadening method and Fourier transform. The fanout beam intensity uniformity is optimized to within ±10% and the packing density is 2.5 delay lines/cm^2.

II SYSTEM DESIGN

The 2-D substrate guided wave optical elements are used for successive optical delays of up to $32\Delta\tau$. Figure 3 illustrates the basic system architecture of our 5-bit device. A 1-to-4 fiber beam splitter with pre-determined output fiber lengths is used to provide four delay signals, each with eight $\Delta\tau$ delay increment. Each of the delay signal from the 1-to-4 bream splitter is coupled into the substrate surface-normally with a specific substrate bouncing angle through a holographic coupler and is then zig-zagging within the substrate through total internal reflection (TIR)[17,18]. Portions of the substrate guided waves are sequentially extracted surface-normally through a holographic output coupler array. Figure 4 illustrates the structure of one of the four TTD sub-unit with delay paths provided by

cascaded substrate guided optical fanouts. The input holographic grating coupler is designed to couple the surface normal incoming light into a substrate guided mode. The output holographic grating couplers extract an array of substrate guided beams into a free-space one-dimensional (1-D) array having 8 surface normal fanout beams. Different optical delays are obtained at subsequent fanouts within the substrate. Equivalent delay intervals are obtained at subsequent fanouts due to equivalent propagating distance difference. The time delay between two successive collinear fanouts is $\Delta\tau$. Thus, 32 (2^5) delay lines are achieved. The fanout optical signals are detected by high speed photodetector array and then sent to antenna transmitters by programmed switching.

Each of such true-time-delay unit can be used not only to provide true-time-delay signals to one antenna element but also to provide delay signals to several antenna elements simultaneously. In the first case, let's suppose that the PAA is programmed to steer from +45° to -45° angular range. For the 5-bit TTD unit, the smallest differential delay increment is given by[14]

$$\Delta\tau = L\sin\Phi_{max} / 31c, \tag{2}$$

where L is the linear dimension of the linear PAA. Assume L =65cm, then $\Delta\tau$ = 50 ps.

In the second case, as shown in Figure 2, 36 antenna elements are divided into 9 groups. Each subarray is controlled by one delay signal. A phase shifter is behind each antenna element. Similarly, suppose the PAA is programmed to steer from +45° to -45° angular range and L = 67 cm. The scanning angle and the corresponding delay of each subarray are shown in Table 1, where $\Delta\tau$ is set as 50 ps.

Table 1 Scanning angles and the corresponding delays of each subarray

Scanning angle	Subarray 1	Subarray 2	Subarray 3	Subarray 4	Subarray 5	Subarray 6	Subarray 7	Subarray 8	Subarray 9
-45°	0	4Δτ	8Δτ	12Δτ	16Δτ	20Δτ	24Δτ	28Δτ	32Δτ
-32°	0	3Δτ	6Δτ	9Δτ	12Δτ	15Δτ	18Δτ	21Δτ	24Δτ
-21°	0	2Δτ	4Δτ	6Δτ	8Δτ	10Δτ	12Δτ	14Δτ	16Δτ
-10°	0	Δτ	2Δτ	3Δτ	4Δτ	5Δτ	6Δτ	7Δτ	8Δτ
0°	0	0	0	0	0	0	0	0	0
10°	8Δτ	7Δτ	6Δτ	5Δτ	4Δτ	3Δτ	2Δτ	Δτ	0
21°	16Δτ	14Δτ	12Δτ	10Δτ	8Δτ	6Δτ	4Δτ	2Δτ	0
32°	24Δτ	21Δτ	18Δτ	15Δτ	12Δτ	9Δτ	6Δτ	3Δτ	0
45°	32Δτ	28Δτ	24Δτ	20Δτ	16Δτ	12Δτ	8Δτ	4Δτ	0

With a substrate total internal bouncing angle of θ, the optical delay between successive output couplers is given by

$$\Delta\tau = \frac{\Delta L'}{c/n} = \frac{2d/\cos\theta}{c/n}, \qquad (3)$$

where $\Delta L'$ is the difference in propagation length between two successive fanouts, d is the substrate thickness, c is the speed of light, and n is the refractive index of the substrate material[14]. For a 50ps delay, one possible thickness d of the quartz substrate is 3 mm, the corresponding θ is 53.5° and the distance between two successive fanouts is 8 mm.

The TTD architecture reported herein offers the compactness and wide instantaneous bandwidth outperformance any existing TTD lines, including the guided-wave TTD lines. The potential advantage of integration with detector arrays surface-normally eliminates the delicate interface between the optical delay-lines and the RF switching circuits. Due to the collinear multiplexibility of the delay lines, a high packing density can be achieved. However, the device does have some disadvantages, like high signal loss if one device provides delay signals only to one antenna element because all delays are obtained simultaneously.

III. DEVICE FABRICATION

The input and output holographic couplers can be made from silver halide, dichromated gelatin (DCG) films and from other photopolymer holographic recording films. Here these gratings are created by holographic recording using DuPont photopolymer films (HRF 600X001) due to their achievable high diffraction efficiencies and dry-processing after exposure. The two beam interference method is used to define individual holographic gratings, each at a different recording angle generating a sinusoidal phase modulation profile[18-21]. The 514 nm line from an Argon ion laser is used as the recording wavelength. The laser output is first split into two separate beams, which are spatially filtered and collimated accordingly. Then they are designed to intersect on the photopolymer film with specific angles. These angles determine the grating periodicity and the slanted angle with respect to the surface normal of the film. The substrate bouncing angle depends critically on these two angles. To form a slanted grating coupler that converts a vertical incident wave to a TIR beam with a bouncing angle α in the substrate, the two incident angles of the recording beams with respect to the surface normal of the film are described in Ref [18]. Here the recording and reconstructing parameters are selected so that the Bragg condition is satisfied. Therefore, there is only one diffraction order existing.

Hologram recording procedures on DuPont HRF-600 film consist of recording, UV cure, and a post baking process. HRF 600X001-20 is selected as the recording material because it exhibits a lower scattering loss and a higher diffraction efficiency. The film is 20 mm thick. The hologram recording mechanism in the photopolymer is known to be a three-step process. First, an initial exposure records the interference pattern, which causes the initial polymerization and diffusion of the monomer molecules to bright fringes. A higher concentration of polymerization means a higher refractive index. Second, a uniform UV light is required for dye bleaching and complete polymerization. Third, a baking process is introduced to enhance the index modulation. The maximum refractive index modulation in this type of photopolymer film has been reported to be ~0.04[22], and a large dynamic range of diffraction efficiency as a function of exposure time can also be achieved by adjusting light intensities of the two recording beams.

One common problem related to massive substrate guided optical fanout is that the fanout light intensity drops along the light propagation direction. This is caused by the cascaded fanouts if the output couplers have more or less the same efficiency. Substrate absorption also contributes to the problem. For a practical device, it is desired that the collinear multiplexed beams with true-time-delay paths are uniformly coupled out surface normally. A uniform light intensity will relax the responsivity requirements for wideband fast detectors, hence achieving a well-balanced signal-to-noise(S/N) ratio at the microwave end[14]. This is critical since signal integrity at tens of GHz range is stringently restricted by the S/N ratio requirements and by the limited detector responsivities. To overcome these problems, the coupling efficiencies of the holographic output couplers have to be individually tuned, which is often a challenging task. To ensure a uniform fanout, it is necessary to precisely tune the diffraction efficiency of the kth coupler, k=1, 2..... and N. In general,

$$\eta_k = \frac{\eta_1}{1-(k-1)\eta_1}, \qquad k=1, 2, 3,.....N. \tag{4}$$

Depending on the value of N and the maximum diffraction efficiency achievable for each holographic grating, the diffraction efficiency of each element can be determined. In our case, N=8, and assuming that η_8=90%, diffraction efficiencies for k=1,2, ...7 are determined to be η_1=12.3%, η_2=14%, η_3=16.3%, η_4=19.5%, η_5=24.2%, η_6=32%, η_7=47%.

To achieve the desired diffraction efficiencies, we first derive the relationship governing the diffraction efficiency as a function of the exposure dosage as shown in Figure 5. The holographic output couplers are accordingly recorded with different exposure dosages to achieve desired efficiencies. It is plausible to fabricate the reported device with only two recording processes by tuning the intensity distribution of the recording beams.

IV DEVICE PERFORMANCE EVALUATION

1. Fanout uniformity and loss

As shown in Figure 6, a 1X4 broadband single mode fiber beam splitter with collimators at its output ends is packaged with the fabricated holographic input and output couplers on the substrate. The 4 output beams from the fiber beam splitter are coupled into the substrate by the input couplers on the substrate. Figure 7 shows the image of 5-bit delay fanout lines (4X8) working at a transverse electric (TE) mode and 850 nm with a fanout intensity fluctuation within ±10% as indicated in Figure 8 which shows the relative intensities of the 32 fanouts. The packaging density of the device is 2.5 fanouts/cm^2. From the measured coupling efficiency, the system insertion loss is determined to be 18 dB, including an 8 dB 1X4 fiber beam splitter insertion loss, a 9 dB substrate-guided wave fanout loss, a 1 dB propagation and other loss. Same results can be achieved with signals of a transverse magnetic (TM) mode.

2. Delay step measurement

The delay interval can be measured by employing a Ti:Sapphire femtosecond laser system[16]. Figure 9 illustrates the schematic of measuring the fanout delay intervals. Two successive delay pulses from the TTD unit are combined with a focusing lens and coupled into a multimode fiber. In this way we are guaranteed that the two beams experience equal extra delays after being combined together. The output of the fiber is fed into an ultrafast metal-semiconductor-metal(MSM) photodetector which has a rise time of ~7 ps. The output of the electrical response from the MSM detector is amplified through a 20 GHz 18 dB amplifier and later is connected to a sampling scope. To precisely measure the small time delay (100 ps), sequential equivalent time sampling technique is employed. Since the delay signal is repetitive, samples may be acquired over many repetitions of the signal, with one sample taken on each repetition. When a synchronous trigger is detected, a sample is taken after a very short, but well defined, delay. When the next trigger occurs, a small time increment is added to this delay and the scope takes another scope. This process is repeated many times until the time window is filled. This allows the oscilloscope to accurately capture signals whose frequency components are much higher than the scope's sample rate. As shown in Figure 10, the delay between two successive fanout is 50 ps.

3. Bandwidth measurement

The frequency range of the signals that can be carried by the device, i.e., the bandwidth of the device, is limited by the dispersion among different wavelengths. The dispersion of the device is mainly due to two factors. One is the dispersion caused by hologram grating couplers. Since the diffraction angles of different incident wavelengths are different, the propagation lengths of different wavelengths after n times of bouncing are different.

Therefore, there is a group time delay between different wavelengths. The second factor is material dispersion caused by different phase velocities of different wavelengths. The contribution of these two factors to dispersion can be compensated. The phase delay at total reflection surface is negligible because for different wavelengths, the delays are almost the same. Based on these considerations, we can calculate the dispersion as follows. The group delay τ is given by

$$\tau = \frac{2hmn_1}{\cos\theta_1 \cdot c} - \frac{2hmn_2}{\cos\theta_2 \cdot c} = \frac{2hm}{c}\left(\frac{n_1}{\cos\theta_1} - \frac{n_2}{\cos\theta_2}\right), \tag{5}$$

where h is the height of the substrate, m is the number of zig-zag bounces, c is the velocity of light in free space, and θ_1 and θ_2 are the bouncing angles in the substrate. The period of the signal that can be carried without error should be larger than this group delay. Therefore, the bandwidth is limited. The calculated bandwidth is about 2.0 THz. The bandwidth of the TTD delay unit can be evaluated by measuring the femtosecond laser pulse widths before and after the device[16]. For this purpose, a femtosecond laser pulse is sent through the device. The pulse width of the later fanout beam having the longest propagation distance is measured and then compared with that of the incoming pulse. Fourier transforms are performed on both pulses to deduce the bandwidth of the device. The experimental setup is shown in Figure 11. An argon ion laser (INNOVA-90-PLUS) is used to pump a Ti:Sapphire mode-locked laser (Clark-MXR-model NJA-4) which provides pulses around ~150 fs at the vicinity of 850 nm and the pulse repeats every 10 ns. An autocorrelator (Clark-MXR-model AC-150) which is driven by a computer-interfaced driver module (Clark-MXR-ODL-1E) for calibration and data acquisition is employed to measure the pulse widths before and after entering the TTD device. The time-dependent amplitude of the ultrashort pulse is obtained by the intensity autocorrelation of the pulse itself and a delayed replica. The pulse train is divided into two beams of approximately equal intensity. One beam is directed towards a moving retroreflector which can scan back-and-forth under computer control. The other beam propagates towards a fixed retroreflector. These two retroreflectors redirect each pulse train back onto the beam splitter so that they are combined and directed towards a focusing lens. The lens focuses these two beams into a second-harmonic-generation (SHG) crystal to produce an output that is proportional to the autocorrelation. The range of delays over which the signal is detected is approximately the pulse duration. The autocorrelation integral for an input pulse with intensity distribution of I(t) is given by

$$A(\tau) = \int_{-\infty}^{+\infty} I(t)I(t+\tau)dt, \tag{6}$$

where τ is the time delay. If the difference in length between the two beam paths is Δx, τ is equal to $\Delta x/c$. Assuming that the temporal dependent of the input is Gaussian, this expression becomes

$$A(\tau) \propto I^2 t_0 \exp(-\tau^2 / 2t_0^2), \tag{7}$$

where t_0 is the width of the input pulse. Therefore, by measuring SHG as function of retroreflector position, we can plot the Gaussian curve and determine the pulse width. To minimize any pulse broadening effect caused by the mirrors, two ultrafast mirrors (Newport 10B20UF.25) working at wavelengths ranging from 700nm to 930 nm are used. Figure 12(a) illustrates the autocorrelation traces for the input (reference) and output (dispersed) pulses, respectively. The Fourier transform of the two pulses in frequency domain generates bandwidth information about the device as shown in Figure 12(b). The 3 dB bandwidth of the device is experimentally confirmed to be 2.4 THz which is well-matched with the theoretical prediction.

To testify the wide bandwidth of the device, a 50 GHz optically heterodyned microwave signal is generated, sent through the device, and then measured. Compared with direct modulation of a laser diode (LD) or using external modulators, the broadband microwave signals generated by optical heterodyne techniques provides hundreds of GHz base bandwidth while maintaining high modulation depth. Two tunable diode lasers oscillating at single longitudinal mode are employed to generate 50 GHz signal in our experiment. The outputs from these two lasers with slightly different wavelengths are combined by a 2-to-1 polarization maintaining fiber beam combiner and then sent to wideband photodetector. Suppose that the outputs of these two lasers are given by

$$E_1(t) = A_1 \exp(j\omega_1 t) \tag{8}$$

and

$$E_2(t) = A_2 \exp(j\omega_2 t) = A_2 \exp[j(\omega_1 + \Delta\omega)t], \tag{9}$$

where $\Delta\omega$ is the beat frequency. The output of the photodetector is therefore given by

$$i_d(t) = \frac{e\eta}{h\nu}[A_1^2 + A_2^2 + 2F(\Delta\omega)A_1A_2\cos(\Delta\omega)t], \tag{10}$$

where e is the electron charge, η is the quantum efficiency of the detector, $h\upsilon$ is the photon energy, and $F(\Delta\omega)$ is the frequency response function of photodetector. Due to the limitation of the bandwidths of the detector, amplifier, and the spectrum analyzer, this 50GHz signal can't be detected directly. A third tunable diode laser with wavelength between the above two lasers is used to down-convert this 50 GHz signal to two signals at about 25 GHz. We send this 50 GHz signal directly through the TTD device. The fanout from the device with $32\Delta\tau$ time delay is combined with the output of the third laser and is then sent to ultrafast photodetector with amplifier which is connected to the spectrum analyzer. From the measured signals on Figure 13, we get

$$\Delta\omega=\omega1-\omega2=(\omega1-\omega3)+(\omega3-\omega2)=24.85+25.90=50.75 \text{ GHz}. \tag{11}$$

Presently, 50 GHz is limited only by the frequency response of the amplifier and the spectrum analyzer used. Since a small tune of the laser wavelength (a few Å) will provide a

large beat frequency (tens of GHz), microwave signals as high as several hundred GHz can be readily generated.

V CONCLUSION

A 5-bit true-time-delay lines device having a packing density of 2.5 lines/cm^2 with a minimum delay step of 50 ps is designed, fabricated and demonstrated in this paper. The device is based on a fiber beam splitter in conjunction with substrate-guided wave propagation. The combined collinear fanouts are realized using slanted photopolymer volume phase grating arrays. The 5-bit delay lines are fabricated on 3mm thick quartz substrates with a substrate bouncing angle of 53.5°. The problem of power fluctuation among the outputs due to the cascading fanout effect is experimentally investigated and solved. A power fluctuation controlled to within ±10% among 32 fanouts is achieved. A delay step of 50ps with a 3-dB bandwidth of 2.4 THz is experimentally confirmed. To verify the bandwidth of the device, up to 50GHz optically heterodyned microwave signal is generated, sent through the device, and then detected at the output end. The true-time-delay device presented herein has the potential to be integrated with photodetector arrays to provide a planarized structure on a single substrate together with the surface normal fan-in and fan-out features.

VI ACKNOWLEDGMENTS

This research is sponsored by the Office of Naval Research, the DARPA's Center for Optoelectronics Science and Technology, and the ATP program of the State of Texas. The authors would like to thank Dr. Yoon-Soo Park for his encouragement and support in this project.

VII REFERENCES

[1] J. Frank and W. A. Huting, "Broadband Phased Array concepts", *IEEE Antennas and Propagation International Symposium*, Vol. 2, pp. 1228-1331, 1994

[2] J. J. Lee, R.Y. Loo, S. Livingston, V. Jones, J. Lewis, H. Yen, G. Tangonan, and M. Wechsberg, " Photonic Wideband Array Antennas", *IEEE Transactions on Antennas and Propagation*, Vol. 43, No. 9, pp. 966-982, 1995

[3] E. N. Toughlian and H. Zmuda, "A photonic variable RF delay line for phased array antennas," *IEEE J. of Lightwave Technology*, Vol. 8, no.12 , pp.1824-1828, 1990

[4] R. J. Mailloux, *Phased Array Antenna Handbook*, Artech House, Boston, 1993

[5] W. Ng, A.A. Walston, G.L. Tangonan, J.J. Lee, I.L. Newberg, and N.

Bernstein, "The first demonstration of an optically steered microwave phased array antenna using true-time-delay," *IEEE J. of Lightwave Technology*, Vol. 9, no.9, pp.1124-1131, 1991

[6] H. Zmuda and E. N. Toughlian, *Photonic Aspect of Modern Radar*, Artech House, Boston, 1994

[7] A. Goutzoulis and K. Davies, " All-optical hardware-compressive wavelength-multiplexed fiber optic architecture for true-time delay steering of 2-D phased array antennas", *SPIE*, Vol. 1703, pp.604-614, 1992

[8] L. J. Lembo, T. Holcomb, M. Mickham, P. wisseman, and J. C. Brock, " Low-loss Fiber Optic Time-delay element for Phased-Array Antennas", *SPIE*, Vol. 2155, pp.13-23

[9] W. Ng, D. Yap, A. Narayanan, R. Hayes, and A. Wilston, "A detector-switched GaAs monolithic time-delay network for microwave phased arrays at L and X band", *Topical Meeting on Integrated Photonics Research, IWA4* , pp.418-421, 1993.

[10] C.T. Sullivan, S. D. Mukherjee, M. K. Hibbs-Brenner, and A. Gopinath, " Switched time delay elements based on AlGaAs/GaAs optical waveguide technology at 1.32um for optically controlled phased array antennas", *SPIE*, Vol. 1703, pp.264-271, 1992

[11] E. J. Murphy, T. F. Adda, W. J. Minford, R. W. Irvin, E. I. Ackerman, and S. B. Adams, " Guided-Wave Optical Time Delay Network", *IEEE Photonics Technology Letters*, Vol. 8, No. 4, pp.545-547, 1996

[12] L. H. Gesell, R. E. Feinleib, J. L. Lafuse, and T. M. Turpin, " Acousto-optic control of time delays for array beam steering", *SPIE*, Vol. 2155, pp.194-204, 1994

[13] D. T. K. Tong and M. C. Wu, " A Novel Multiwavelength Optically Controlled Phased Array antenna with a Programmable Dispersion Matrix", *IEEE Photonics Technology Letters*, Vol. 8, No. 6, pp.812-814, 1996

[14] R. T. Chen and R. Lee, "Holographic optical elements (HOEs) for true-time-delays aimed at phased array antenna applications," *SPIE Technical Digest*, vol. 2689, pp.176-187, 1996

[15] R. Li and R. Chen, " 3-bit substrate-guided-mode optical true-time-delay lines operating at 25 GHz", *IEEE Photonics Technology Letters*, Vol. 9, No. 1, pp. 100-102, 1997

[16] R. Li, Z. Fu, and R. Chen, " High density broadband true-time-delay unit on a single substrate", *SPIE* Vol. 3006, pp.256-263, 1997

[17] M. R. Wang, G. J. Sonek, R. T. Chen, and T. Jannson, "Large fanout optical interconnects using thick holographic gratings and substrate wave propagation," *Applied Optics*, vol. 31, no. 2, pp.236-249, 1992.

[18] R. T. Chen, S. Tang, M. Li, D. Gerald, and S. Natarajan, "1-to-12 surface normal three dimensional optical interconnects," *Appl. Phys. Lett.* , vol. 63, no.14, pp.1883-1885, 1993.

[19] J.-H. Yeh and R. K. Kostuk, " Substrate-mode holograms used in

optical interconnects: design issues", *Applied Optics*, Vol. 34, No. 17, pp.3152-3164, 1995

[20] W. J. Gambogi, A. M. Weber, and T. J. Trout, " Advances and Application of DuPont Holographic Photopolymers", *SPIE*, Vol. 2043, pp.2-13, 1993

[21] U. Rhee, J. J. Caulfield, C. S. Vikram, and J. Shamir, " Dynamics of hologram recording in DuPont photopolymer", *Applied Optics*, Vol. 34, No. 5, pp.846-852, 1995

[22] W. J. Gambogi, W. A. Gerstadt, S. R. Mackara, and A. M. Weber, "Holographic transmission elements using improved photopolymer films", *SPIE* Vol. 1555, pp.256-267, 1992

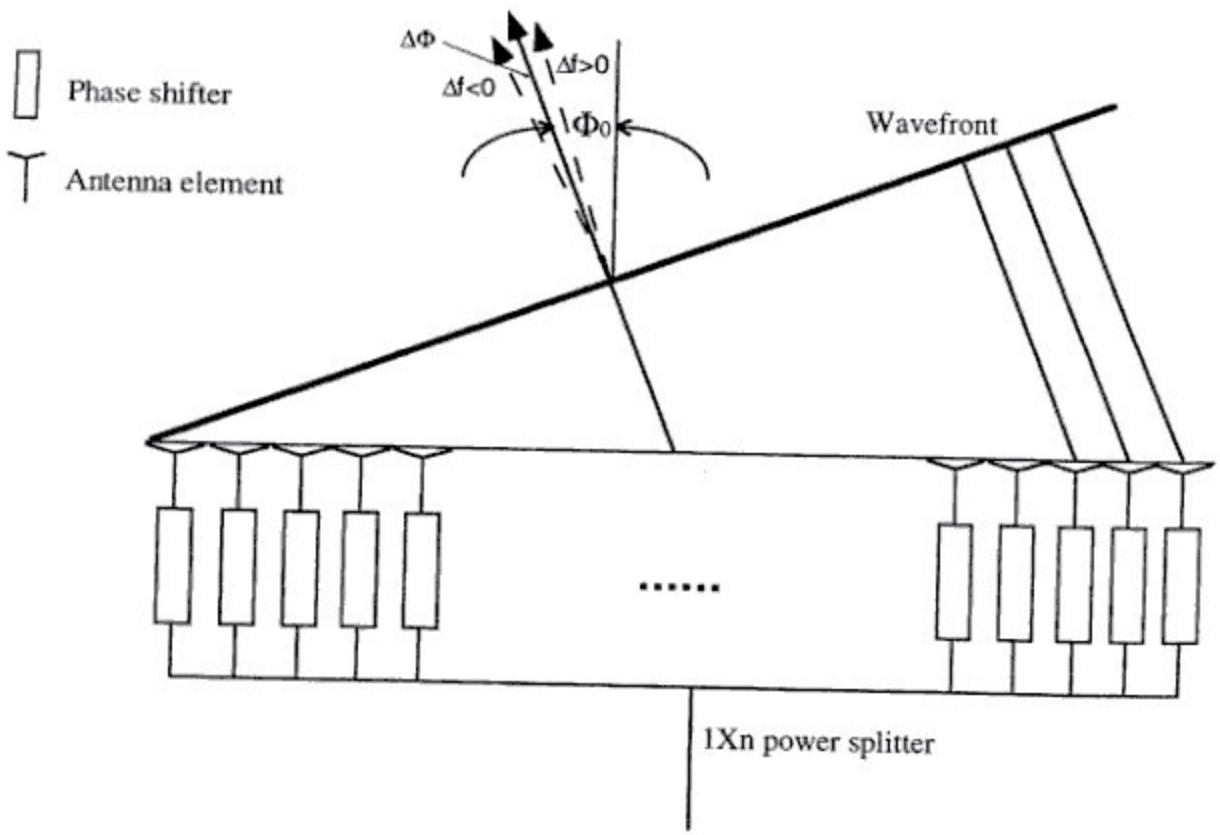

Figure 1. Beam scanning as a result of frequency change

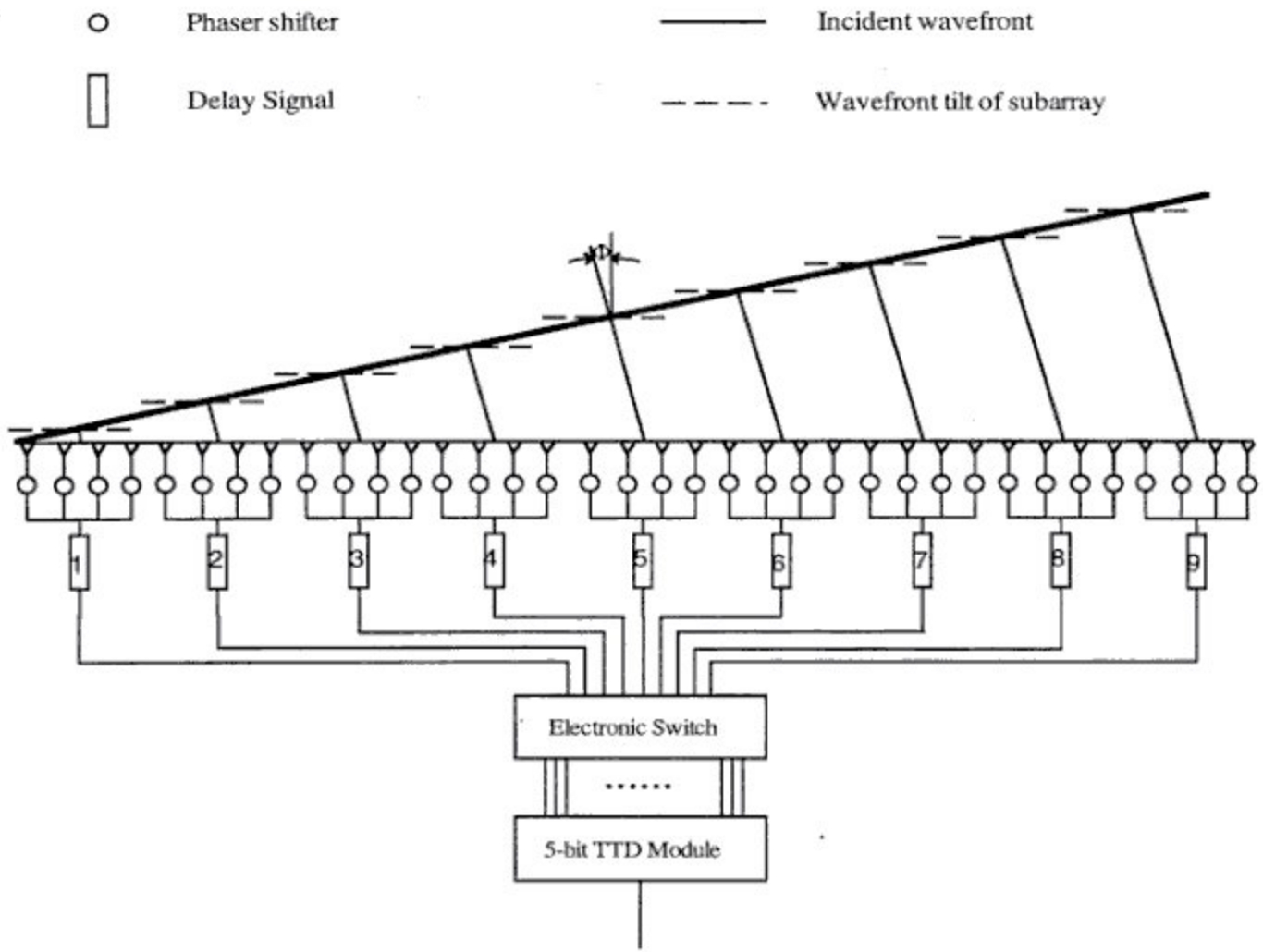

Figure 2. Wide-band scanning array feeds: each unit controls 9 subarrays

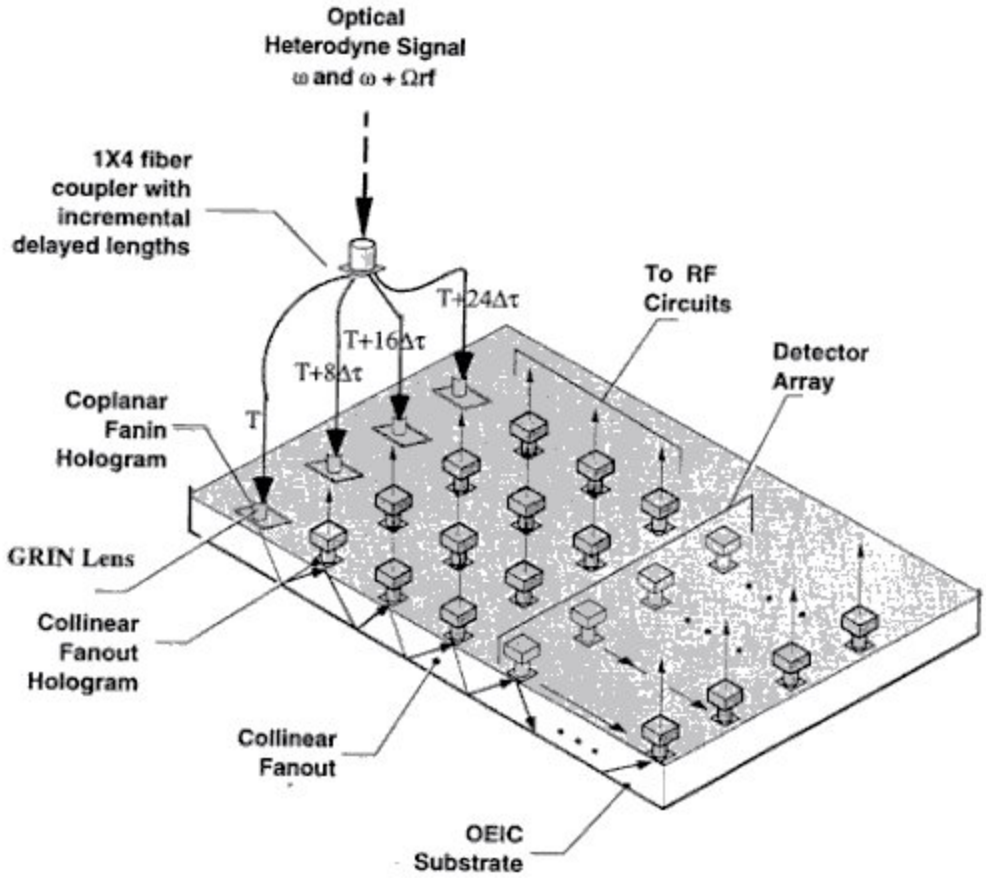

Figure 3. 5-bit optical delay lines based on substrate guided mode with holographic grating couplers

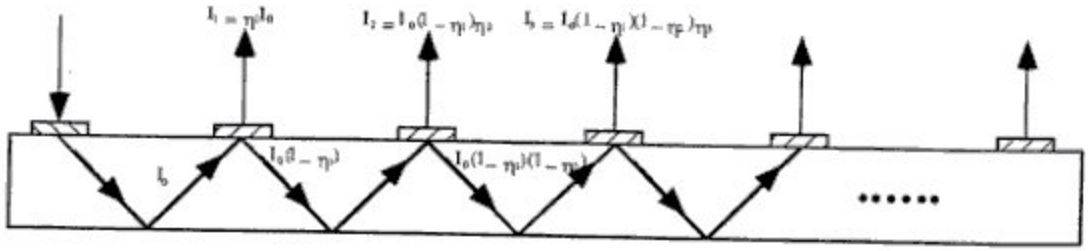

Figure 4. Optical delay lines based on substrate guided mode together with holographic grating couplers

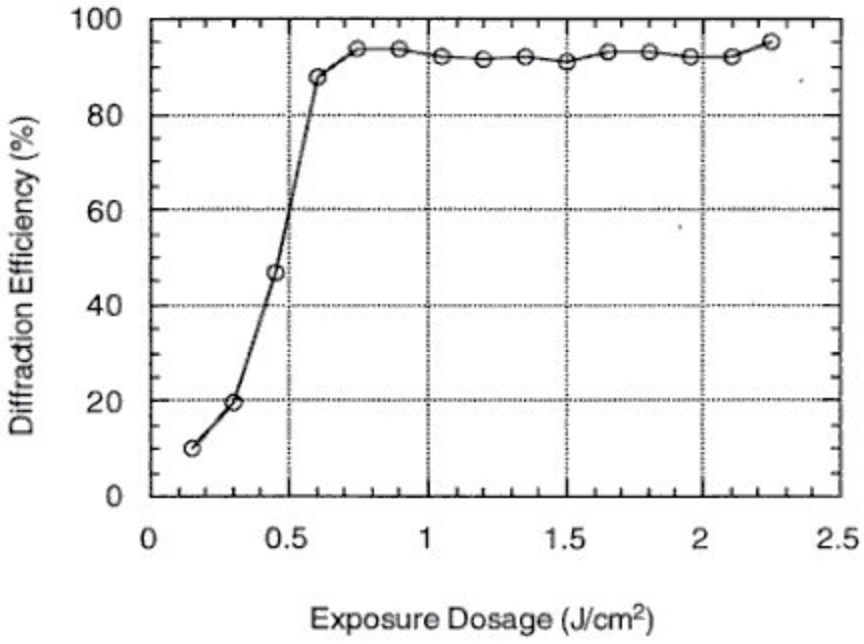

Figure 5. Relation between diffraction efficiency and exposure dosage

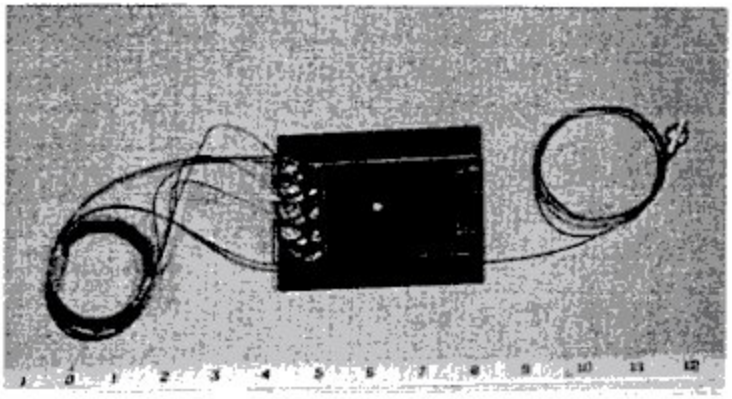

Figure 6. Photograph of the 5-bit TTD module

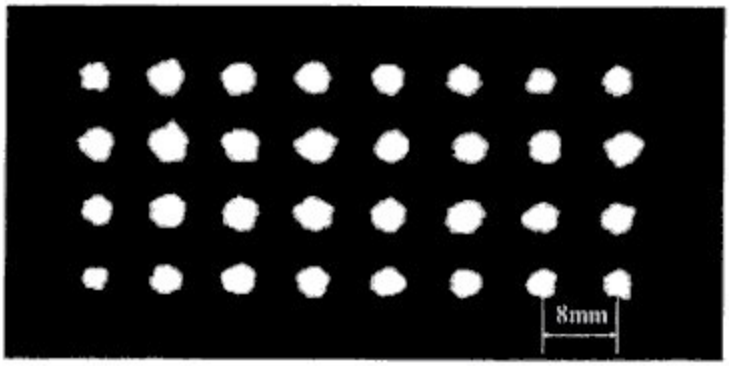

Figure 7. CCD image of 5-bit delay fanout lines (4X8) with a fanout intensity fluctuation within 15%

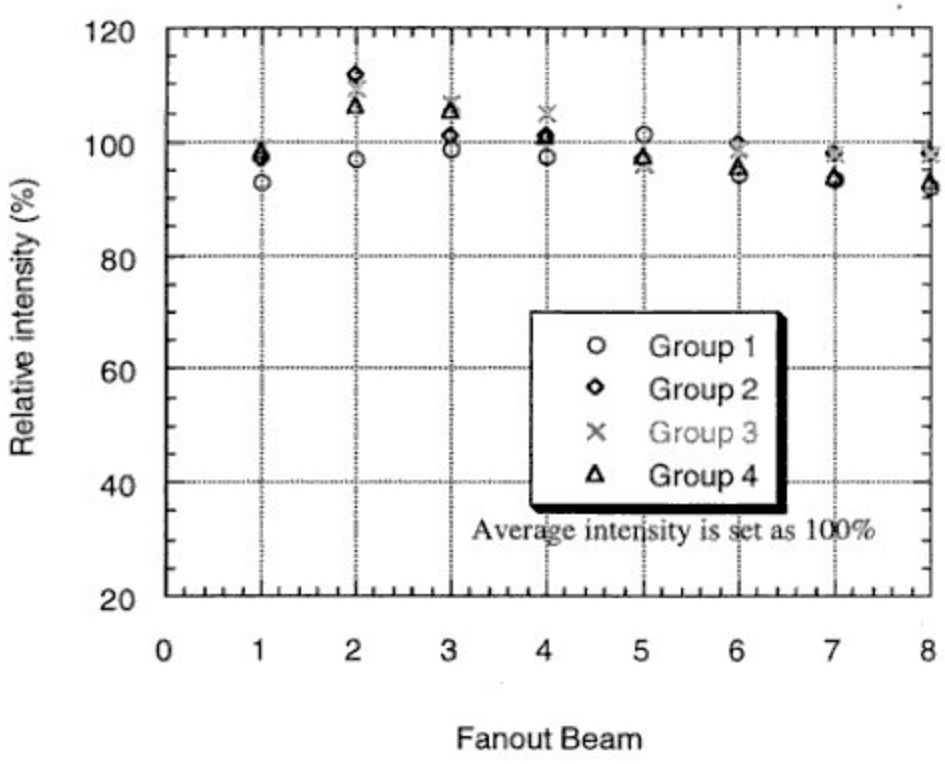

Figure 8. Relative beam intensities of 32 fanouts from the TTD unit

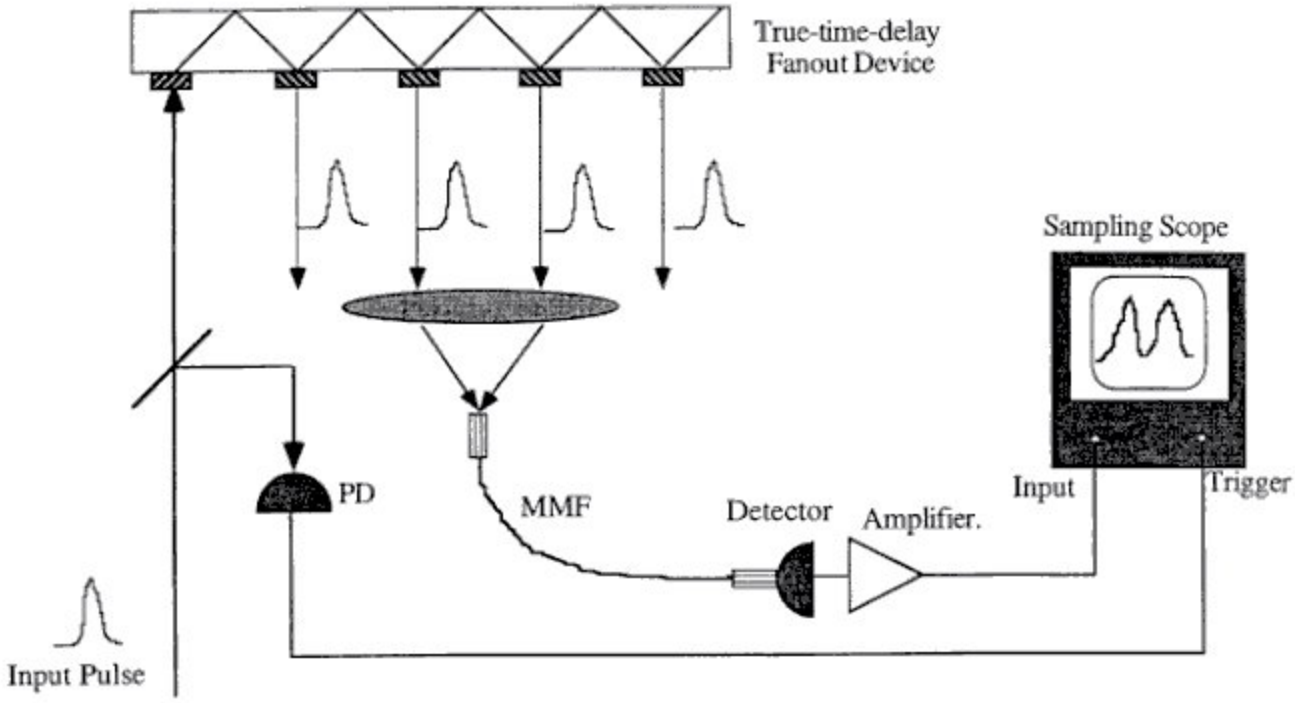

Figure 9 Experimental set-up for measuring the minimum delay interval.

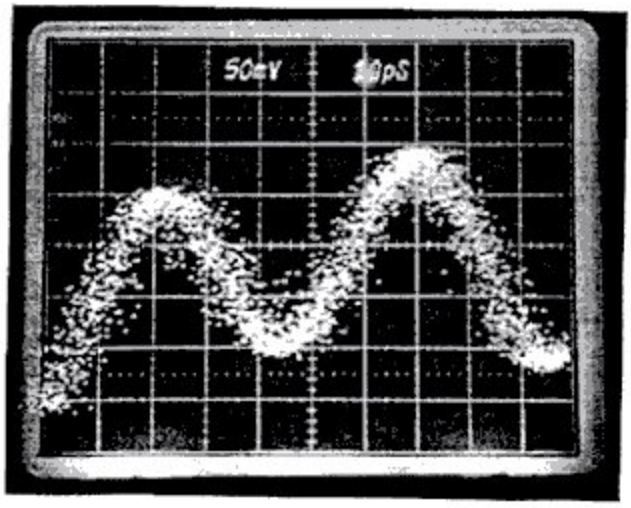

Figure 10. Two pulses coming from successive fanouts with 50ps delay between them

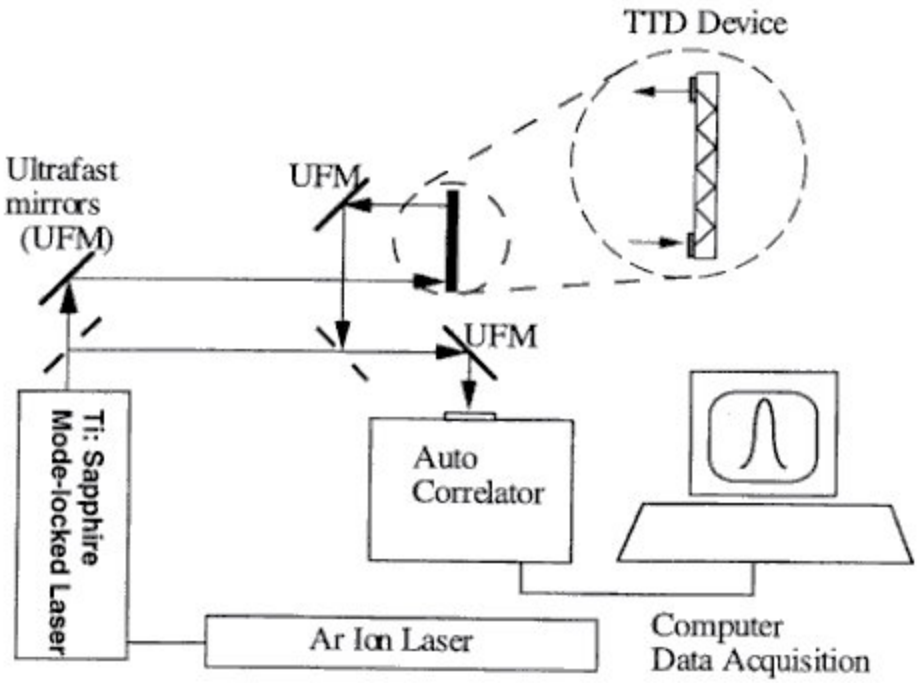

Figure 11. Schematic for measuring the device bandwidth

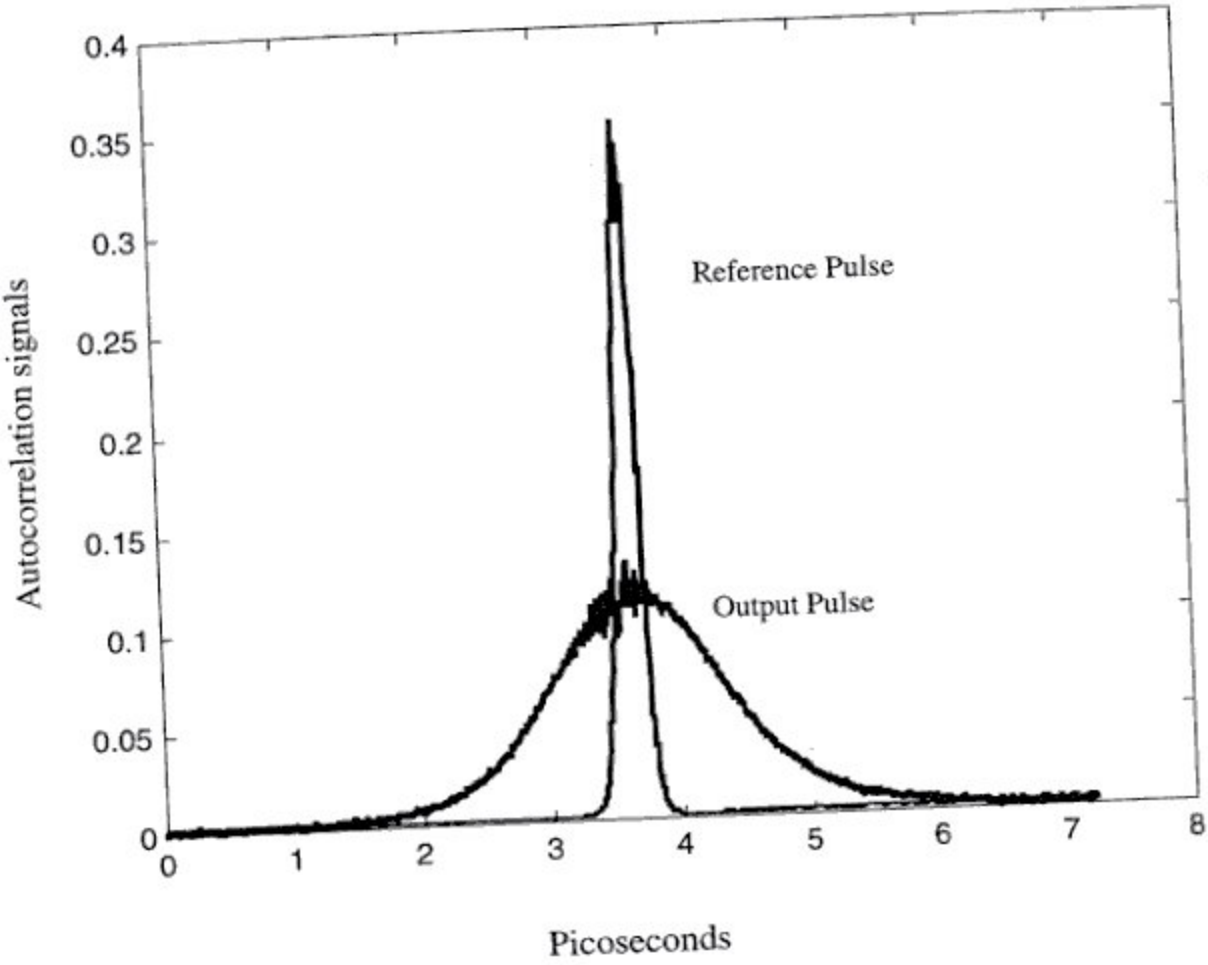

Figure 12(a) Pulse width measured before and after the TTD unit

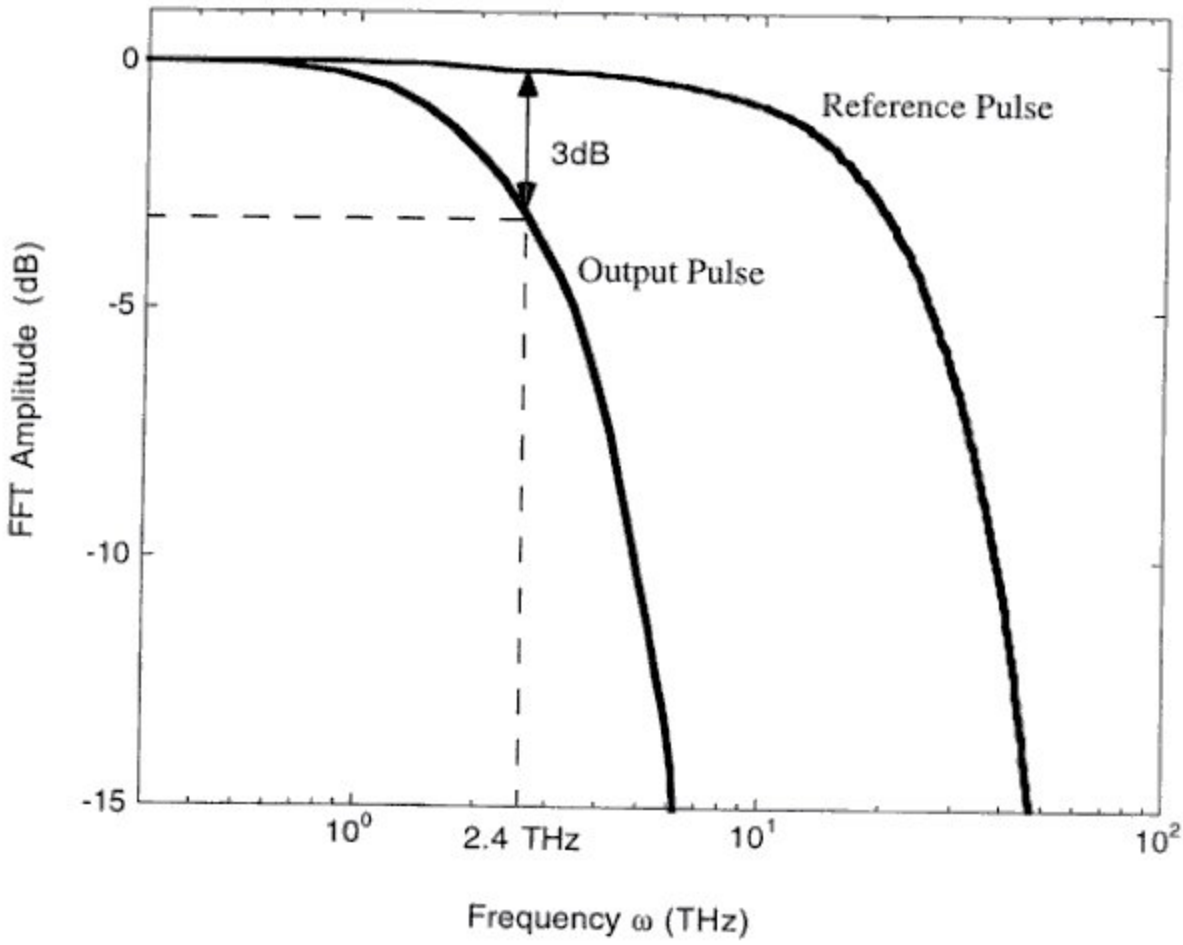

Figure 12(b) FFT power spectrum for the input and output pulses

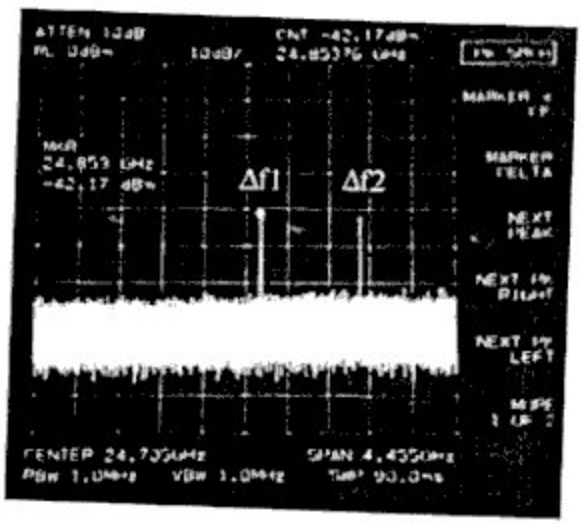

Figure 13. 50 GHz optically heterodyned microwave signal carried by 5-bit TTD module